ACS OMEGA

http://pubs.acs.org/journal/acsodf

Article

Pure Mg−Al Layered Double Hydroxide Film on Magnesium Alloys for Orthopedic Applications

Shi Cheng, Lvqin Lan, Mei Li, Xiao Chu, Hua Zhong,* Mengyu Yao, Feng Peng,* and Yu Zhang*

Cite This: *ACS Omega* 2021, 6, 24575−24584

Read Online

ACCESS | Metrics & More | Article Recommendations | Supporting Information

ABSTRACT: Mg alloys are promising biodegradable orthopedic implants in the future. However, poor corrosion resistance and biocompatibility limit their wide applications. In this study, a pure Mg−Al layered double hydroxide (Mg−Al LDH) film on AZ31 was prepared through combining hydrofluoric acid pretreatment and hydrothermal treatment. Electrochemical analysis and the immersion test suggested that the as-prepared Mg−Al LDH-coated sample exhibited significantly enhanced corrosion resistance. The *in vitro* cell culture revealed that the Mg−Al LDH film was favorable for the alkaline phosphatase activity, collagen secretion, and osteogenesis-related gene expression of MC3T3-E1. Furthermore, the LDH-coated sample was beneficial for the migration, vascular endothelial growth factor secretion, and angiogenesis-related gene expression of human umbilical vein endothelial cells. The subcutaneous implantation test demonstrated that the Mg−Al LDH film could protect the substrate from corrosion and induce milder inflammation. The femur implantation demonstrated that the Mg−Al LDH sample showed better bone regeneration and osseointegration than bare AZ31. In summary, the as-prepared pure Mg−Al LDH film is able to enhance the *in vitro* and *in vivo* performances of AZ31, indicating a promising application in the orthopedic field.

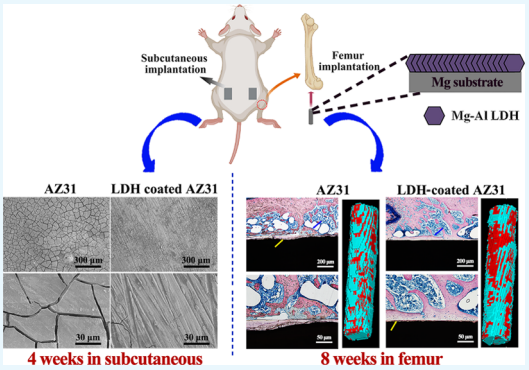

1. INTRODUCTION

Mg alloys are widely used in various fields such as the automotive industry, electronic products, aerospace industry, and biomedical implants because of their exceptional properties such as low density, good electromagnetic shielding characteristics, high damping capacity, high rigidity, and biodegradability.[1−3] However, the low electrochemical potential of Mg alloys results in poor corrosion resistance, which inhibits their large-scale applications, especially in the biomedical field. The fast corrosion of Mg implants leads to the formation of gas cavity, loss of mechanical support, acute inflammatory reaction, and so on.[4−6]

Layered double hydroxides (LDHs) have received increased attention for their facile fabrication and effective corrosion protection in the past decade.[7] The LDHs, also known as anionic clay or hydrotalcite, are composed of positively charged brucite-like layers and a negatively charged interlayer region. Their chemical formula is $[M^{2+}_{1-X}M^{3+}x(OH)_2][A^{n-}]_{x/n}\cdot zH_2O$, where M^{2+} represents bivalent cations, such as Mg^{2+}, Zn^{2+}, or Ni^{2+}, and M^{3+} represents trivalent cations such as Al^{3+}, Fe^{3+}, or Mn^{3+}.[8,9] Owing to the tunable structure of LDHs, many different types of LDHs (Mg−Al, Mg−Fe, Mg−Cr, Ni−Al, and Zn−Al) containing various interlayer anions (NO_3^-, CO_3^{2-}, Cl^-, and VO_3^-) were fabricated on the surface of Mg alloys via hydrothermal treatment.[10−16] In some of these studies, not only the corrosion resistance was evaluated, but also the biocompatibility of the LDH films was investigated. For example, Lin et al. found that human mesenchymal stem cells exhibited better spreading and proliferation on a Mg−Fe LDH-coated Mg substrate.[11] Among these different types of LDH films, Mg−Al LDH has been the widest studied owing to its easy fabrication. Researchers have investigated the influence of the pH value, reaction temperature, and substrate microstructure on the formation of the Mg−Al LDH film and the corresponding corrosion resistance.[17−19] In addition, new methods (mainly steam coating) and pretreatment (mainly anodic oxidation) were also proposed to prepare the Mg−Al LDH film on Mg alloys.[20−23] Although these studies were devoted to prepare a pure Mg−Al LDH film on Mg alloys, almost all the prepared Mg−Al LDH films were mixed with a $Mg(OH)_2$ phase, which can be ascribed to the fast release of Mg^{2+} from the substrate during the reaction process. Only Han et al. successfully developed a pure Mg−Al LDH film on Mg alloys using a complicated and time-consuming method.[24,25] According to their study, carbonic acid was prepared by bubbling CO_2 (solution A) and an Al source was

Received: June 17, 2021
Accepted: August 17, 2021
Published: September 16, 2021

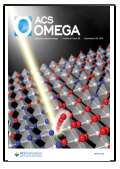

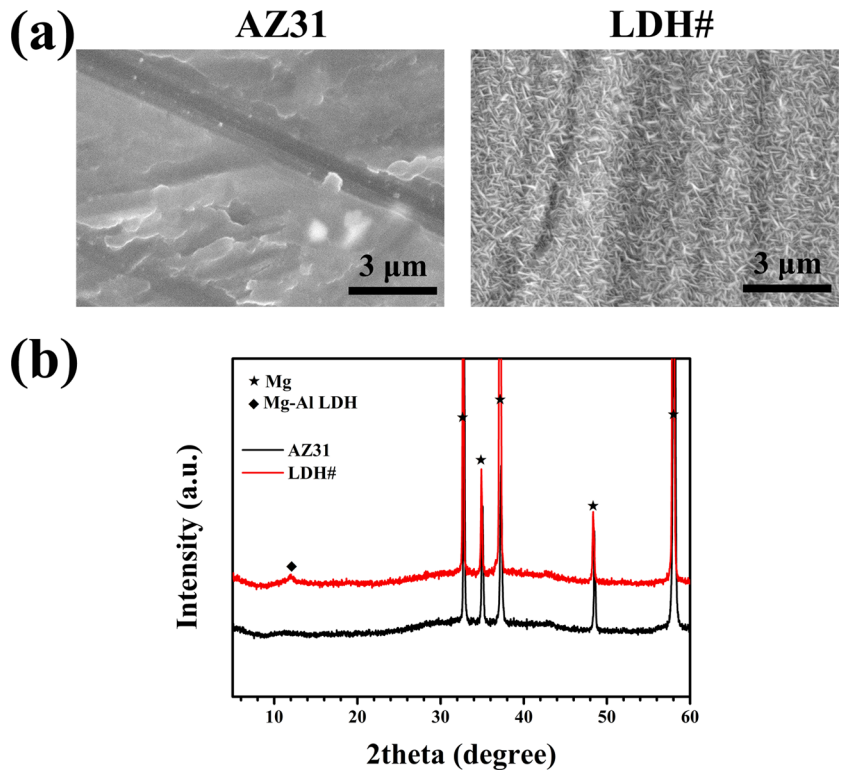

Figure 1. Surface morphologies (a) and XRD patterns (b) of AZ31 and LDH# samples.

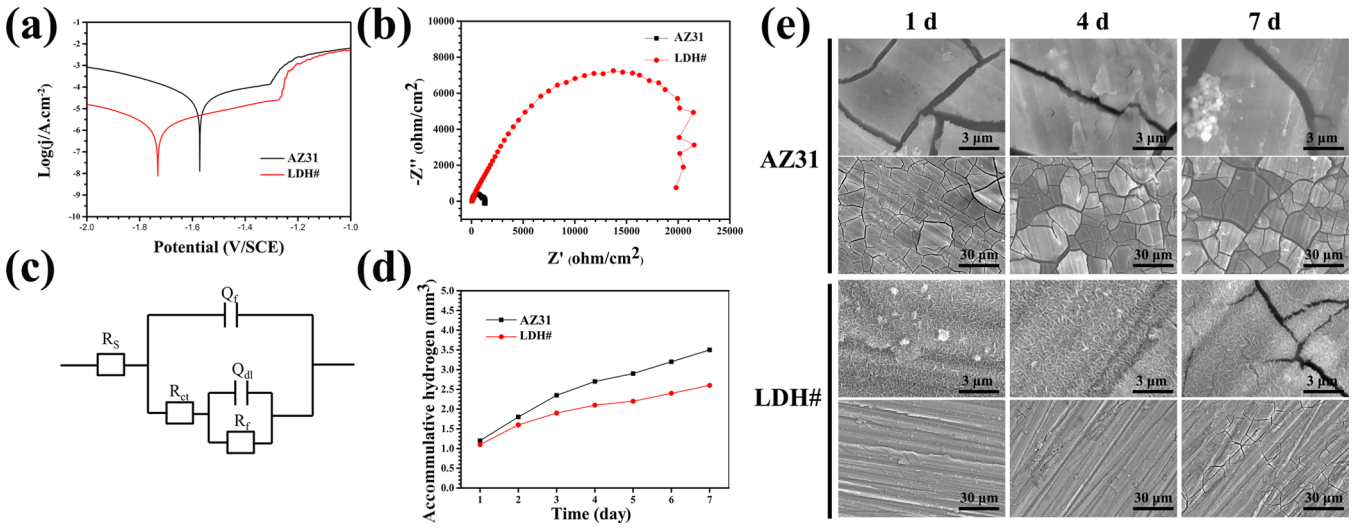

Figure 2. Potentiodynamic polarization (a) and EIS (b) results of AZ31 and LDH#; equivalent circuit of EIS results (c); R_s is the solution resistance; Q_f and R_f are the capacitance and resistance of the corrosion production or coating on AZ31, respectively; R_{ct} and Q_{dl} are the charge-transfer resistance and the constant phase element of the electrical double layer, respectively; and accumulative hydrogen evolution (d) and surface views (e) of AZ31 and LDH# samples after being immersed in PBS.

prepared by dissolving a pure Al plate in a Na_2CO_3 solution (solution B). Solution B was then added into solution A, and the pH value of the mixed solution was adjusted to 10.5 using NaOH. Finally, the reaction solution was obtained. To broaden the application of Mg−Al LDH on the Mg substrate, it is highly important to design a new facile and time-saving method to fabricate a pure Mg−Al LDH film on Mg alloys.

In this study, a pure Mg−Al LDH film was formed on the surface of the AZ31 alloy via a two-step method. The MgF_2 conversion film was first formed on the AZ31 alloy using hydrofluoric acid treatment, and the as-obtained MgF_2 was then transferred to Mg−Al LDH (the final sample was denoted as LDH#) using hydrothermal treatment. *In vitro* and *in vivo* corrosion resistance, histocompatibility, and osteogenesis ability of the as-prepared pure Mg−Al LDH film were investigated.

2. RESULTS AND DISCUSSION

2.1. Coating Characterizations. The surface views of the AZ31 alloy and LDH# samples are shown in Figure 1a. Some scratches were observed on the surface of the AZ31 alloy, which were ascribed to the process of grounding using SiC

https://doi.org/10.1021/acsomega.1c03169
ACS Omega 2021, 6, 24575−24584

paper. The surface of the LDH# sample was uniformly deposited with micro−nano flakes, which are the typical morphologies of the Mg−Al LDH film.[15] The X-ray diffraction (XRD) patterns are exhibited in Figure 1b. Only Mg feather peaks at approximately 12, 18, 38, and 58° were detected for the AZ31 sample. For the LDH# sample, in addition to the characteristic peaks of Mg, a peak at 12° indicated the existence of Mg−Al LDH (JCPDS no. 50-1684). No feather peak at 18° was detected, revealing that the formed Mg−Al LDH was a pure phase without $Mg(OH)_2$ impurity.

There have been many literature studies dedicated to fabricate LDH films on Mg alloys.[7] However, owing to the fast release of Mg^{2+} from the substrate, the LDH film formed was accompanied by $Mg(OH)_2$ impurity. Although the surface of the Mg alloy was pretreated to control the release of Mg^{2+} (such as anodic oxidation), the presence of $Mg(OH)_2$ impurity was inevitable.[20] Therefore, a new pretreatment was required to control the release of Mg^{2+}. In this study, we used hydrofluoric acid treatment as pretreatment for three reasons: (1) hydrofluoric acid treatment is a commonly used method for the pretreatment of Mg alloys[26] because the presence of the MgF_2 passive film can improve its corrosion resistance; (2) few F elements are good for the biological performance of Mg-based implants because proper F ions exhibit favorable antibacterial properties and induce bone formation properties;[27] and (3) more importantly, the solubility product (K_{sp}) of MgF_2 is higher than that of $Mg(OH)_2$ (5.16×10^{-11} *vs* 5.61×10^{-12} at 25 °C) according to the Handbook of Inorganic Chemicals. A higher K_{sp} value of MgF_2 indicates that MgF_2 would gradually convert to $Mg(OH)_2$ (reaction 1), which is the predecessor of Mg−Al LDH. Therefore, the formation of a pure Mg−Al LDH film is possible by controlling the formation of $Mg(OH)_2$.

$$MgF_2 + 2OH^- \rightarrow Mg(OH)_2 + 2F^- \quad (1)$$

In this study, the MgF_2 film gradually dissolved and released proper Mg^{2+} to form Mg−Al LDH, and finally, a pure Mg−Al LDH film was obtained.

2.2. Corrosion Resistance and Biocompatibility of the Pure Mg−Al LDH Film. The potentiodynamic polarization curves are shown in Figure 2a, and the calculated values of corrosion potential (E_{corr}), corrosion current density (j_{corr}), and corrosion resistance (R_p) are illustrated in Table 1. The E_{corr} value of the LDH# sample was lower than that of the AZ31 sample, which was also observed by other researchers.[28] The j_{corr} value of LDH# (9.72×10^{-7} A/cm^2) was 2 orders lower than that of AZ31 (2.4×10^{-5} A/cm^2), and the R_p value was 2 orders higher than that of AZ31, suggesting that the Mg−Al LDH film can effectively protect the substrate. Numerous studies have prepared the Mg−Al LDH film on Mg alloys; however, because of the existence of the $Mg(OH)_2$ phase, their j_{corr} values are higher than the j_{corr} value in this study. For example, Anjum et al. fabricated a coating with Mg−Al LDH and $Mg(OH)_2$ mixed phases on AZ31, and the sample exhibited a j_{corr} value of 6.74×10^{-6} A/cm^2;[29] Kuang et al. reported a Mg−Al LDH and $Mg(OH)_2$ mixed phase coating on pure Mg using a two-step method, and the modified sample exhibited a j_{corr} value of 4×10^{-5} A/cm^2.[30]

Table 1. Corrosion Data of AZ31 and LDH# Samples

	E_{corr} (V)	j_{corr} (A/cm^2)	R_p (Ω/cm^2)	R_{ct} (Ω/cm^2)
AZ31	−1.58	2.24×10^{-5}	5.40×10^4	74.61
LDH#	−1.73	9.72×10^{-7}	1.39×10^6	561.60

Electrochemical impedance spectroscopy (EIS) was also applied to analyze the corrosion behavior of the samples, and the result is presented in Figure 2b. The LDH# sample showed significantly larger impedance than AZ31 did. The fitted electrical circuit can be illustrated as $R_s[Q_f\ (R_f\ (Q_{dl}\ R_{ct}))]$ (Figure 2c), where R_{ct} represents the reaction resistance, and the calculated values of R_{ct} are shown in Table 1. The R_{ct} value of the LDH# sample was approximately 7.6 times that of the AZ31 sample. These electrochemical results revealed that the LDH# sample possessed a better corrosion resistance than the AZ31 sample. To further evaluate the performance of the as-prepared LDH film, the samples were immersed in phosphate-buffered saline (PBS) for 7 days. The amount of hydrogen released and surface views are shown in Figure 2d,e, respectively. Hydrogen released from the LDH# sample was less that from the AZ31 sample, indicating that the substrate of the LDH-coated sample suffered from less corrosion. Furthermore, the accumulative release of Mg ions (Figure S1) from the samples was consistent with the result of hydrogen evolution. Many cracks were observed on the surface of AZ31 at day 1, indicating severe corrosion (Figure 2e). However, no cracks were observed on the surface of the LDH# sample until day 4. Some cracks appeared on the LDH# sample after being immersed for 7 days, but the number of the cracks is less and the width is narrower than that on the AZ31 sample. This suggested that the Mg−Al LDH film can effectively resist the attack of the corrosive medium.

Good cytocompatibility is a crucial parameter for implant biomaterials. Figure 3a demonstrates the early adhesion morphology of MC3T3-E1. No cells were observed on the surface of AZ31 at three detected time points. However, the spreading cells were observed on the LDH# surface after culturing for 1 h. The spreading area of the cells increased along with time, and a numerous amount of filopodia and lamellipodia were detected at 24 h. Figure 3b shows the fluorescence images of MC3T3-E1 after being cultured for 3 days. A few dead cells and no living cells were detected on the surface of AZ31. However, living cells were covered on the surface of the LDH# sample. Even by culturing for 7 and 14 days, a large number of living cells covered the surface of the LDH# sample (Figure S2). The cytocompatibility of the sample extracts was also evaluated, and the result is demonstrated in Figure 3c. The cells cultured in the extract of AZ31 exhibited cell viability below 70% at days 3 and 5, indicating severe cytotoxicity. However, when cultured in the extract of LDH#, the cell viability was nearly 100%. A pure Mg−Al LDH film on AZ31 is suitable for cells to adhere and proliferate on its surface, and no cytotoxicity was found in its extract, suggesting a good biocompatibility.

In our previous study, a film composed of Mg−Al LDH and $Mg(OH)_2$ was found to significantly enhance the corrosion resistance of the JDBM alloy.[15] This was because the Mg−Al LDH could resist the attack of chloride ions via anion exchangeability.[31,32] However, the cells showed poor adhesion and proliferation in such a film, indicating that a more protective film was needed. Hence, we focused on fabricating a pure Mg−Al LDH film on the Mg alloy. In this work, the as-prepared pure Mg−Al LDH-coated AZ31 showed significantly higher corrosion resistance compared to bare AZ31. For bare AZ31, poor corrosion resistance means that a large amount of Mg ions is released from the substrate, resulting in the increase

https://doi.org/10.1021/acsomega.1c03169
ACS Omega 2021, 6, 24575−24584

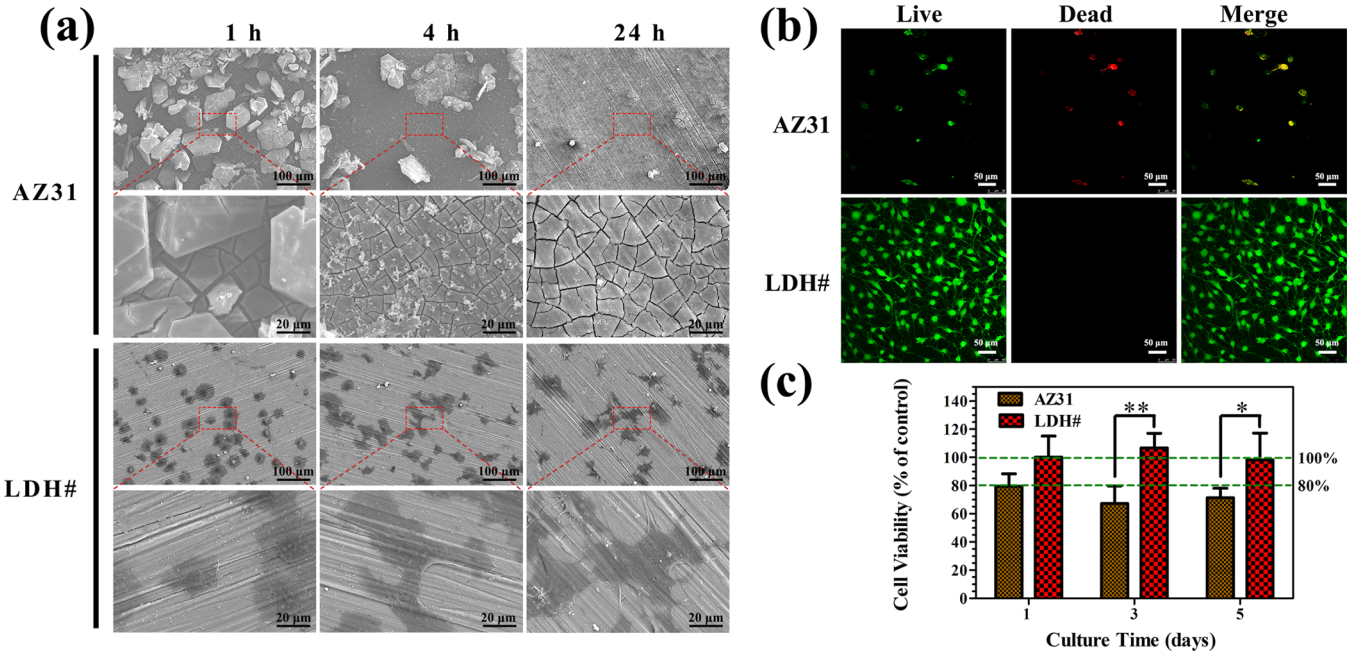

Figure 3. SEM images of MC3T3-E1 after being cultured on AZ31 and LDH# samples for 1, 4, and 24 h (a); live/dead staining images of MC3T3-E1 after being cultured on AZ31 and LDH# for 3 days (b), green represents living cells and red represents dead cells; and cell viability of MC3T3-E1 after being cultured in the extracts of AZ31 and LDH# for various durations (c).

of osmotic pressure. Meanwhile, a large amount of hydroxyl ions released from the substrate cause a sharp increase in the pH value. In the synergistic effects of the high osmotic pressure and pH value, cells cannot keep alive on the AZ31 surface. For LDH-coated AZ31, a favorable corrosion resistance means a milder osmotic pressure and pH value, so cells can keep alive and proliferate on its surface. Moreover, the nanostructure is reported to be favorable for cell adhesion and spreading.[33] The LDH# was covered by micro−nano flake structures, which is also beneficial for the cell adhesion.

2.3. *In Vitro* Osteogenic Differentiation and Angiogenesis Ability Evaluations. Alkaline phosphatase (ALP) activity and COL secretion are vital markers for the osteogenic differentiation of stem cells. For both the markers, larger and strongly stained areas were observed for the LDH# group (Figure 4a). In addition, the osteogenic differentiation was evaluated at a molecular level. Figure 4b displays the expression level of osteogenesis-related genes of MC3T3-E1. For all the detected genes, the cells cultured in the LDH# extract exhibited a significantly higher expression than those in the AZ31 extract. Especially for the OCN expression, the LDH# group was almost 6 times as much as that of the AZ31 group. Results of ALP activity, COL secretion, and bone-related gene expression suggested that the pure Mg−Al LDH-coated sample was more favorable for the osteogenic differentiation of MC3T3-E1.

In the past few years, extensive literature studies have revealed that angiogenesis is also important for new bone regeneration because a matured vasculature can sufficiently supply the required materials (such as nutrients, circulating cells, and oxygen) for bone growth.[34−36] In this study, the angiogenic behavior of human umbilical vein endothelial cells (HUVECs) was evaluated by culturing in the extracts of AZ31 and LDH# samples. The cell viability of HUVECs is presented in Figure 5a. After being cultured for 1 day, the cells showed a significantly higher viability in the LDH# extract. After being

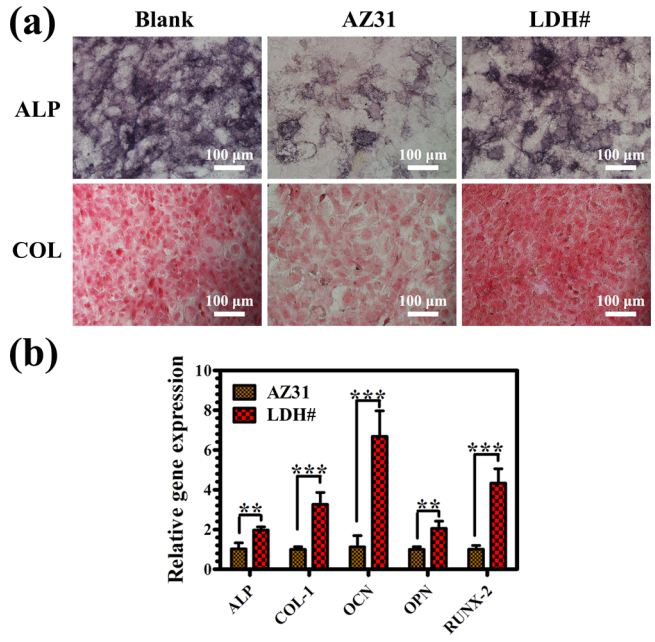

Figure 4. ALP-positive areas and COL secretion of MC3T3-E1 cultured in various extracts (a) and expression of osteogenesis-related genes in MC3T3-E1 cultured in various extracts (b).

cultured for 4 and 7 days, the viability of the cells in the LDH# extract was still higher than that in the AZ31 extract, but no statistical differences were detected. The migration of HUVECs is a vital step for the formation of blood vessels. In this study, the migration of HUVECs was evaluated using a scratch assay (Figure 5b). A cross line with a width of 540 ± 10 μm was drawn by pipet tips. After culturing for 12 h, the cells cultured in AZ31 and LDH# extracts evidently migrated into the drawn area and left gaps of 343 ± 8 and 182 ± 5 μm, respectively, indicating a better HUVEC migration for the

https://doi.org/10.1021/acsomega.1c03169
ACS Omega 2021, 6, 24575−24584

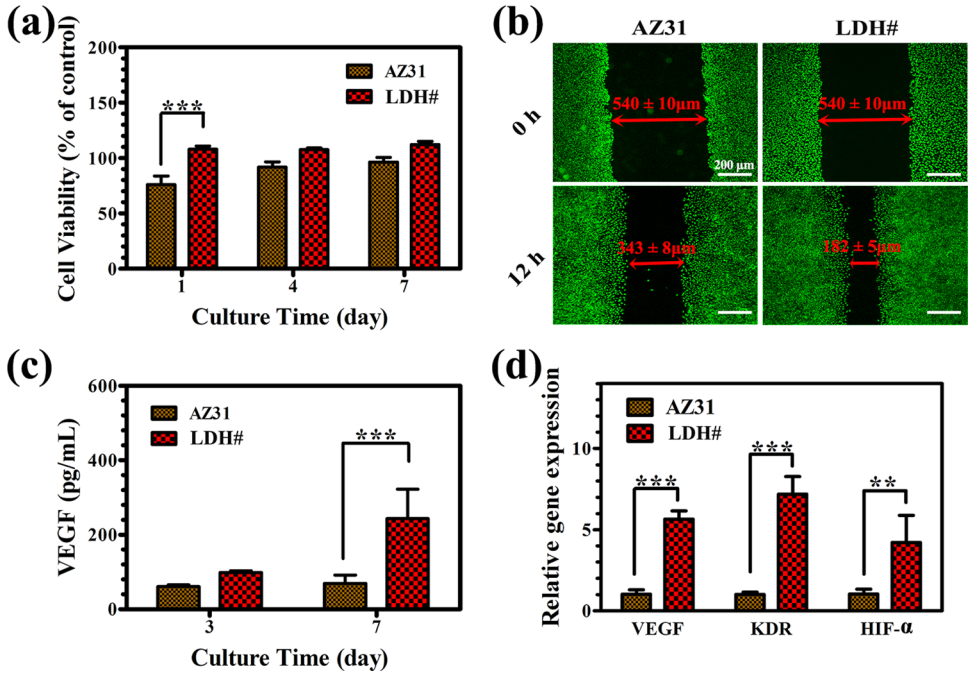

Figure 5. Cell viability (a), migration (b), VEGF protein levels (c), and angiogenesis-related gene expression (d) of HUVECs cultured in various extracts.

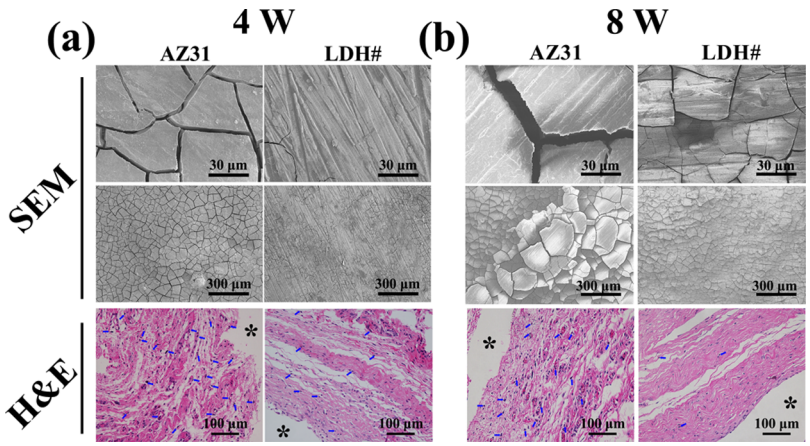

Figure 6. SEM views of the corroded surface and photomicrographs of the histological section of AZ31 and LDH# samples after subcutaneous implantation for 4 (a) and 8 weeks (b).

LDH# group. The vascular endothelial growth factor (VEGF) is a vital factor which plays an important role in the migration, proliferation, and vessel formation process of HUVECs. The secretion of VEGF protein was detected by enzyme-linked immunosorbent assay (ELISA), and the result is displayed in Figure 5c. At day 3, HUVECs cultured in the LDH# extract secreted more VEGF proteins than those cultured in the AZ31 extract, but no statistical difference was detected. At day 7, the secreted VEGF level for the LDH# group was significantly higher than that for the AZ31 group. Additionally, the expression level of angiogenesis-related genes was also detected (Figure 5d). The expressions of VEGF, KDR, and HIF-α gene for HUVECs cultured in the LDH# extract were 4.6, 6.2, and 3.2 times higher than those cultured in AZ31 extracts, respectively. The results of ELISA and the real-time polymerase chain reaction (RT-PCR) verified the enhanced angiogenic behaviors of the pure Mg−Al LDH-coated sample at a molecule and gene level.

As revealed by the electrochemical and immersion tests (Figure 2), Mg−Al LDH-modified AZ31 exhibited a significantly better corrosion resistance. Therefore, the LDH# sample showed less Mg ion release and a milder increase of the pH value. A suitable amount of Mg ions and pH value are favorable for the cell adhesion, spreading, and proliferation (Figure 3) and thus guarantee the favorable osteogenesis- and angiogenesis-inducing capabilities of the LDH# sample.

2.4. *In Vivo* Evaluations. Subcutaneous implantation was applied to evaluate the *in vivo* corrosion resistance and histocompatibility of AZ31 and LDH# samples, and the results are presented in Figure 6. After being implanted for 4 weeks (Figure 6a), cracks were evenly distributed on the surface of AZ31, while only few cracks were observed on the surface of the LDH# sample. Notably, the LDH structures were retained on the surface of LDH# (Figure S3a). After being implanted for 8 weeks (Figure 6b), the width of cracks on AZ31 appeared to be larger than that at week 4 (8.6 ± 0.7 *vs* 4 ± 0.5 μm). A

https://doi.org/10.1021/acsomega.1c03169
ACS Omega 2021, 6, 24575−24584

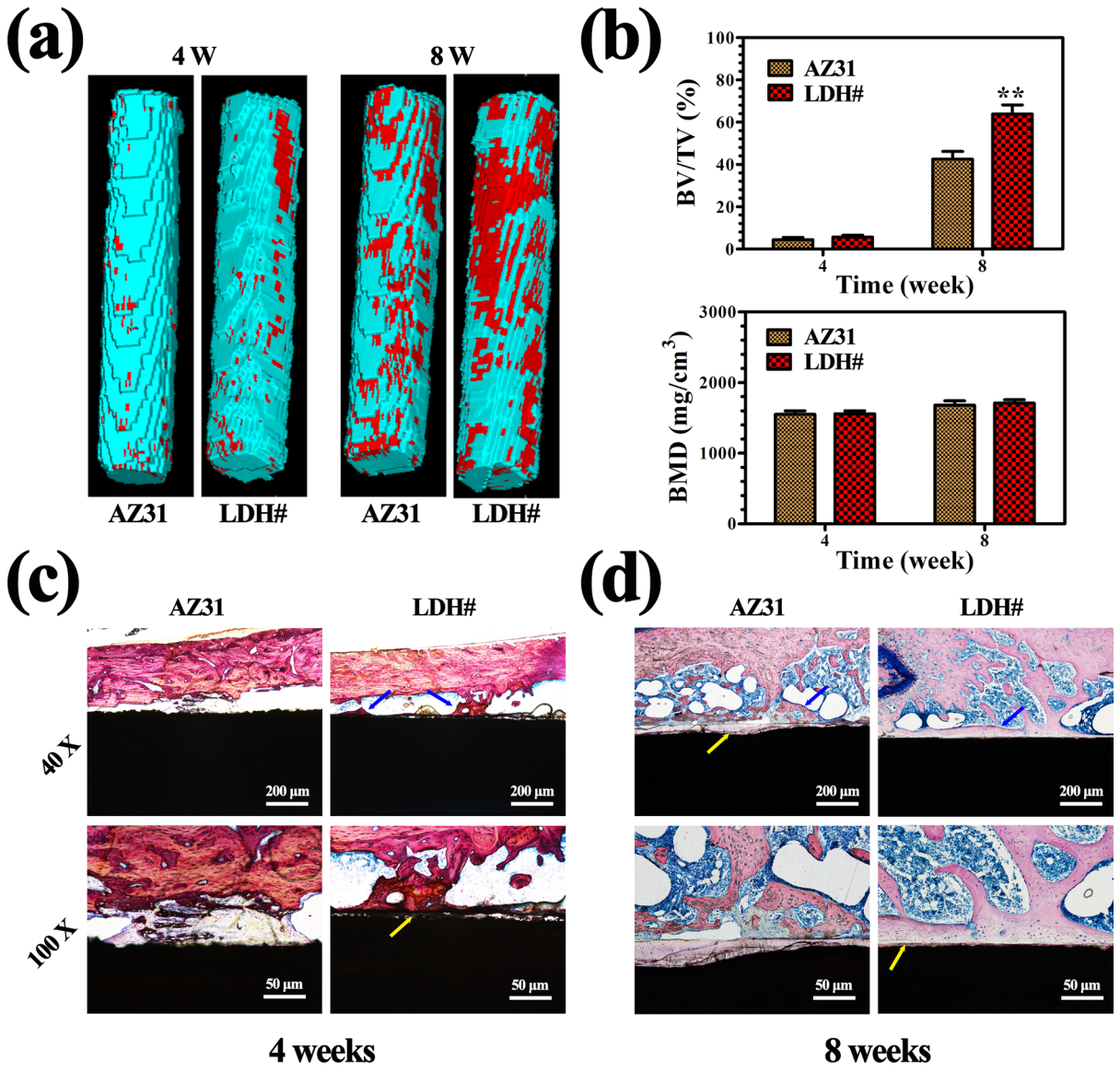

Figure 7. 3D reconstruction images of micro-CT results (a), red sections indicate new bones; calculated *BV/TV* and trabecular BMD (b); and VG staining of AZ31 and LDH# samples after femur implantation for 4 weeks (c) and 8 weeks (d), blue arrow indicates the newly formed bone and yellow arrow indicates the corrosion product.

more number of cracks were observed on the LDH# surface, but the width of cracks was narrower than that on AZ31 at week 4 (1.4 ± 0.2 *vs* 4 ± 0.5 μm), suggesting improved *in vivo* corrosion resistance by the Mg−Al LDH film. In addition, LDH structures were also maintained on the surface (Figure S3b), revealing a good stability of LDH structures *in vivo*. At week 4, the hematoxylin and eosin (H&E) staining result suggested that both the samples would induce a local inflammation response (verified by neutrophils), but the LDH# group was milder than the AZ31 group. At week 8, numerous neutrophils were detected on the tissue of the AZ31 group, while only a few neutrophils were observed on the tissue of the LDH# group. These results revealed that the inflammation reaction caused by AZ31 cannot be eliminated by host healing ability, but the inflammation reaction caused by the LDH# sample can be healed after 8 weeks, indicating a favorable *in vivo* histocompatibility.

Femur implantation was carried out to evaluate the osteointegration capability of AZ31 and LDH# samples. Figure 7a illustrates the reconstructed three-dimensional (3D) micro-CT images. The calculated bone volume/tissue volume (*BV/TV*) and bone mineral density (BMD) values are presented in Figure 7b. The new bone volume was visually larger for the LDH# group than for the AZ31 group at both weeks 4 and 8. However, the quantitative analysis of the BT/TV value showed that there was no significant difference observed between AZ31 and LDH# groups at week 4. Nevertheless, the BT/TV value of the LDH# group was higher than that of the AZ31 group at week 8. As for the value of BMD, no significant difference was detected at both weeks 4 and 8. Many studies have proved that bare Mg implants show a higher BMD value than Ti implants.[37,38] In this study, Mg ions would release from both AZ31 and LDH# implants, so the BMD values of the two groups were in the same level. Furthermore, according to our previous study, the concentration of Mg ions in the range of 3.125−25 mM can improve cell viability, while once the concentration exceeds 25 mM, it would suppress cell viability.[39] A large amount of Mg ions released from the AZ31

https://doi.org/10.1021/acsomega.1c03169
ACS Omega 2021, 6, 24575−24584

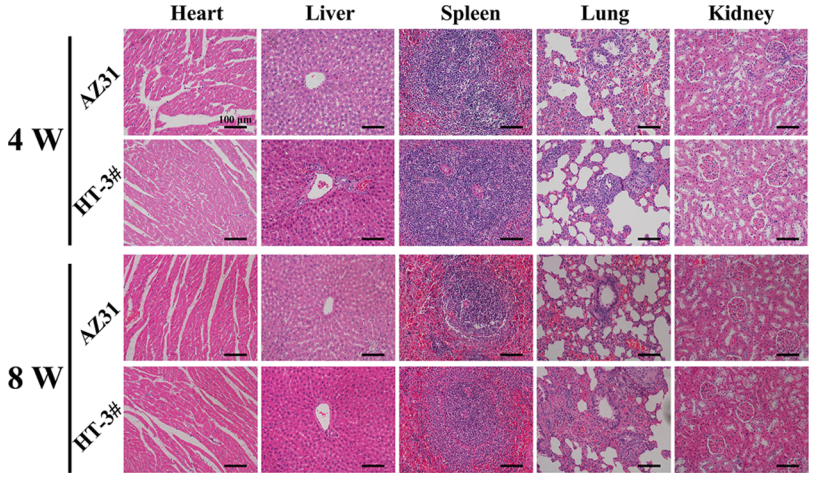

Figure 8. Typical histological morphology of important organic tissues in the H&E sections of AZ31 and LDH# samples after femur implantation for 4 and 8 weeks.

implant would do harm to cell viability, and thus, the AZ31 implant showed a lower BV/TV value than the LDH# implant in this study.

Figure 7c,d represents the histological sections of AZ31 and LDH# groups stained with Van Gieson's (VG) solution. At week 4, few newly formed bones were observed surrounding the AZ31 implant. However, newly formed bones can be detected surrounding the LDH# implant, but the bone (indicated by blue arrows) was discontinuous and corrosion products (indicated by yellow arrows) were observed in the gap between the new bone and the implant. Notably, the surface of AZ31 displayed a more serious corrosion morphology with many cracks (Figure S4), representing a poorer corrosion resistance in femur than that in the LDH# implant. At week 8, a new bone grew into the marrow cavity for the AZ31 group. However, no new bone was detected near the surface of the implant, but a layer of corrosion products was detected. In the case of the LDH# group, a great degree of continuous newly formed bone was directly bonded with the surface, indicating a superior osteointegration. These results suggested that the pure Mg−Al LDH film on AZ31 improved its osteogenesis and osteointegration ability. The H&E staining of different organs after femur implantation for 4 and 8 weeks is represented in Figure 8. For both AZ31 and LDH# groups, no pathological changes were observed in the heart, liver, spleen, lung, and kidney, indicating favorable biosafety of both the implants.

For biodegradable metals, the *in vivo* performances are mainly decided by their corrosion behaviors. Hence, for the LDH# implant, because it showed enhanced corrosion resistance, a milder inflammation reaction in subcutaneous and a better osteointegration in femur were prospective.

3. CONCLUSIONS

In this work, pure Mg−Al LDH-coated AZ31 was fabricated by combining hydrofluoric acid pretreatment and hydrothermal treatment. The Mg−Al LDH-coated sample exhibited better *in vitro* corrosion resistance and was more suitable for the osteogenic differentiation of MC3T3-E1 and vascularization of HUVECs. Subcutaneous implantation suggested that Mg−Al LDH could protect the AZ31 substrate from severe corrosion and induce a mild host inflammation response. Femur implantation suggested that Mg−Al LDH-coated AZ31 showed enhanced osseointegration. In summary, with enhanced corrosion resistance, biocompatibility, and osteointegration, the novel and simple *in situ* method to fabricate pure Mg−Al LDH films on Mg alloys shows a promising potential for orthopedic applications.

4. MATERIALS AND METHODS

4.1. Sample Preparation and Characterization. Commercially purchased AZ31 alloys (ChuanMao Metal material Co., Ltd., Suzhou) were used as substrates. The AZ31 alloys were immersed in a hydrofluoric acid solution (40 v/v%; Sinopharm Chemical Reagent Co., Ltd., Shanghai) for 6 h. Subsequently, the hydrofluoric acid-treated AZ31 alloys were placed in a Teflon-lined stainless-steel container. The reaction solution was 0.02 M $Al(NO_3)_3$ (pH = 12.8 adjusted by NaOH), and the stainless-steel container was kept at 120 °C for 12 h. The obtained samples were denoted as LDH#.

The surface morphology was observed using scanning electron microscopy (SEM; Hitachi-S3400N, Hitachi, Japan). The phase compositions were detected using XRD (D/Max, RIGAKU, Tokyo, Japan) with Cu Kα radiation (40 kV, 30 mA).

4.2. Corrosion Evaluation. The corrosion resistance of the samples was evaluated by an electrochemical analyzer (CHI760C; Shanghai, China) in PBS. Potentiodynamic polarization and impedance spectra tests were both carried out in a three-electrode electrochemical cell. The exposure area of the sample to the electrolyte was 0.255 cm^2. The samples were stabilized in PBS to obtain a stable open-circuit potential before the test. The potentiodynamic polarization test was performed at a scanning rate of 10 mV/s. The values of E_{corr}, j_{corr}, and R_p were determined using the Tafel extrapolation. The impedance spectra test was performed by applying a 5 mV sinusoidal perturbing signal and recorded from 100 kHz to 10 mHz. ZView software was used to analyze the result.

The AZ31 alloy and LDH# samples were put in 400 mL beakers (four specimens of each group in one beaker), and 360 mL of PBS was then added. The hydrogen released was collected using inverted funnels and was recorded every day for 7 days. The corrosion morphologies of the samples after being immersed in PBS for 1, 4, and 7 days were observed by SEM.

4.3. *In Vitro* Cytocompatibility. *4.3.1. Cell Culture.* Osteoblast-like cells (MC3T3-E1, Cells Resource Center of

https://doi.org/10.1021/acsomega.1c03169
ACS Omega 2021, 6, 24575−24584

Shanghai Institute for Biological Science, Shanghai, China) and HUVECs (ScienceCell, USA) were used. MC3T3-E1 was cultured in the α-minimum essential medium (α-MEM) containing 10% fetal bovine serum (FBS, Hyclone, USA) and 1% antimicrobial penicillin/streptomycin mixture (P/S, Hyclone, USA). HUVECs were cultured in the endothelial cell medium (ECM) containing 10% FBS, 1% P/S, and 2.5% VEGF (Hyclone, USA). Cells were incubated at 37 °C in a 5% CO_2 incubator. The samples were sterilized by ultraviolet radiation before use.

4.3.2. Cell Adhesion. The samples were placed in 24-well plates and added with 1 mL of cell suspension containing 5×10^4 cells. After 1, 4, and 24 h incubation, the culture media were removed, and the samples were rinsed three times with PBS. Subsequently, the wells were added with 2.5% (v/v) glutaraldehyde and kept at 4 °C overnight. The cells were then dehydrated and then observed using SEM.

4.3.3. Live-Dead Staining. The cells were cultured on the AZ31 alloy and LDH# samples for 3 days. Then, the cells were rinsed three times with PBS and then added with 100 μL of dyeing solution (5 μM propidium iodide and 2 μM calcium-AM, Sigma, USA). After being cultured for another 15 min, the cells were rinsed with PBS and kept in PBS. The cells were observed using confocal laser scanning microscopy (Leica SP8, Germany).

4.3.4. Cell Viability in Extracts. The extracts of different samples were obtained by immersing the samples in the culture media (α-MEM and ECM) for 24 h with an area−volume ratio of 1.25 cm^2/mL. α-MEM or ECM was used as positive control groups. 100 μL of MC3T3-E1 or HUVEC suspension with 5×10^3 cells was added to 96-well plates. After being cultured for 1 day, the culture media were replaced with various extracts and incubated for another 1, 3, and 5 days. The Alamar Blue assay (AbD Serotec Ltd., UK) was applied to evaluate the cell viability according to the manufacturer's instruction.

4.4. *In Vitro* Osteogenic Differentiation of MC3T3-E1.

4.4.1. Alkaline Phosphatase Activity and Collagen Secretion. MC3T3-E1 was cultured on various extracts for 7 days. The cells were fixed with 4% paraformaldehyde, and then, ALP activity staining was applied with AS-MX phosphate, fast blue RR salt, and Mayer's hematoxylin solution. Images were captured using a phase-contrast inverted optics microscope.

For collagen (COL) detection, the cells were fixed with 4% para-formaldehyde and stained with 0.1% Sirius Red. The stained cells were pictured using an optics microscope.

4.4.2. Quantitative RT-PCR Analysis. The gene expressions, including ALP, type-1 COL , osteocalcin, osteopontin, and runt-related transcription factor 2, were measured on MC3T3-E1 after being cultured for 7 days. Total RNA was isolated using a Trizol reagent (Invitrogen, CA, USA). After quantifying the concentration using nanodrop 2000 (Thermo-Fisher, USA), the acquired RNA was reverse transcribed into cDNA using the 1st Strand cDNA synthesis supermix Kit (Yeasen, China). Furthermore, the cDNA was analyzed by RT-PCR using SYBR Green Mastermix (Yeasen, China) and primers. The running program of RT-PCR included an initial denaturation period of 1.5 min at 95 °C, 40 cycles at 95 °C for 15 s, and at 60 °C for 30 s. GAPDH was selected as a housekeeping gene. The primer sequences are listed in Table S1.

4.5. *In Vitro* Angiogenic Behavior of HUVECs.

4.5.1. Cell Migration. HUVECs were seeded on the 24-well plate at a density of 1×10^5 cells/well. After being cultured for 1 day, lines were drawn across the cell layer using 200 μL pipet tips and then added various extracts. After another 8 h, the cells were fixed with 4% paraformaldehyde, permeabilized with 0.1% Triton X-100, stained with rhodamine−phalloidin and DAPI, and observed using a fluorescence microscope (Olympus IX 71, Olympus, Japan).

4.5.2. Quantification of VEGF Protein Secretion. HUVECs were seeded on the 24-well plate at a density of 2×10^4 cells/well. After 4 h, the culture media were replaced with various extracts and incubated for 3 and 7 days. After that, the secretion of VEGF protein was quantified using the ELISA kit (Abcam, USA) according to the manufacturer's instruction.

4.5.3. Quantitative RT-PCR Analysis. The gene expressions of the kinase insert domain receptor, hypoxia-inducible factor 1-alpha (HIF-α), and VEGF of HUVECs were measured according to Section 4.4.2. The primer sequences are listed in Table S1.

4.6. Animal Experiment. All the animal experiments were approved by the Animal Care and Use Committee of Guangdong General Hospital. Sprague-Dawley rats (5-week old; adult male) were used.

4.6.1. Subcutaneous Implantation. Eight rats were anesthetized by intraperitoneal injection of pentobarbital sodium (40 mg/Kg). The skin on the back was shaved and sterilized with 2% iodine. Two pockets were sliced on each rat on their bilateral back and then implanted with the samples. Four rats were sacrificed at 4 weeks, and the others were sacrificed at 8 weeks.

The surface morphologies of the implanted samples were viewed using SEM. The tissues surrounding the implants were collected and fixed with paraformaldehyde, dehydrated, embedded in paraffin, and stained with H&E to evaluate the inflammatory reaction.

4.6.2. Femur Implantation. Eight rats were anesthetized by intraperitoneal injection of pentobarbital sodium (40 mg/Kg). The lateral sides of the knee joints were carefully exposed via skin incision and muscle blunt dissection. Holes (Φ 2 mm) were predrilled longitudinally into femur, and the materials were then implanted. The wound was closed in layers and injected with prophylactic antibiotics consecutively for 3 days. The bilateral femurs were harvested at 4 and 8 weeks after implantation. Furthermore, tissues, including heart, liver, spleen, lung, and kidney, were collected and fixed in 4% paraformaldehyde. The obtained tissues were dehydrated, embedded in paraffin, and stained with H&E.

The harvested femurs containing implants were scanned using Micro-CT (Quantum FX, PerkinElmer), and more than 500 layers were imaged at the implanted site. Multimodal 3D Visualization (Siemens, Germany) software was used to reconstruct the 3D images. VG Studio MAX software was used to calculate the *BV/TV* and the BMD.

After micro-CT imaging, the femur specimens were dehydrated using gradient ethanol, embedded in polymethylmethacrylate, cut into longitudinal sections (100 μm) using a saw microtome (EXAKT Apparatebau, Germany), and then ground and polished to a final thickness of approximately 50 μm. The polished sections were stained with VG solution and visualized using an optics microscope.

4.7. Statistical Analysis. All data are presented as mean ± standard deviation. Statistical analyses were performed using one-way ANOVA, followed by using Tukey's post hoc test via SPSS 19.0 software. Statistical significance was confirmed when the *P*-value was < 0.05.

https://doi.org/10.1021/acsomega.1c03169
ACS Omega 2021, 6, 24575−24584

■ ASSOCIATED CONTENT

Supporting Information

The Supporting Information is available free of charge at https://pubs.acs.org/doi/10.1021/acsomega.1c03169.

Primer sequence of tested genes in quantitative RT-PCR; accumulative release of Mg ions from AZ31 and LDH# samples; live/dead staining images of MC3T3-E1 after being cultured on AZ31 and LDH# for 7 and 14 days; surface morphology of the LDH# implant after subcutaneous implantation for 4 and 8 weeks; and surface morphology of AZ31 and LDH# implants after femur implantation for 4 weeks (PDF)

■ AUTHOR INFORMATION

Corresponding Authors

Hua Zhong − *The Fifth Affiliated Hospital of Southern Medical University, Guangzhou 510920, China*; Phone: 86-13760776599; Email: zhong8099@163.com

Feng Peng − *Department of Orthopedics, Research Center of Medical Sciences, Guangdong Provincial People's Hospital, Guangdong Academy of Medical Sciences, Guangzhou, Guangdong 510080, China*; orcid.org/0000-0003-2366-2253; Phone: 86-18616936841; Email: peng_feng7@163.com

Yu Zhang − *Department of Orthopedics, Research Center of Medical Sciences, Guangdong Provincial People's Hospital, Guangdong Academy of Medical Sciences, Guangzhou, Guangdong 510080, China; The Second School of Clinical Medicine, Southern Medical University, Guangzhou 510515, China*; Phone: 86-13602744495; Email: zhangyu@gdph.org.cn

Authors

Shi Cheng − *Department of Orthopedics, Research Center of Medical Sciences, Guangdong Provincial People's Hospital, Guangdong Academy of Medical Sciences, Guangzhou, Guangdong 510080, China*

Lvqin Lan − *Department of Orthopedics, Research Center of Medical Sciences, Guangdong Provincial People's Hospital, Guangdong Academy of Medical Sciences, Guangzhou, Guangdong 510080, China*

Mei Li − *Department of Orthopedics, Research Center of Medical Sciences, Guangdong Provincial People's Hospital, Guangdong Academy of Medical Sciences, Guangzhou, Guangdong 510080, China*

Xiao Chu − *Department of Orthopedics, Research Center of Medical Sciences, Guangdong Provincial People's Hospital, Guangdong Academy of Medical Sciences, Guangzhou, Guangdong 510080, China*

Mengyu Yao − *Department of Orthopedics, Research Center of Medical Sciences, Guangdong Provincial People's Hospital, Guangdong Academy of Medical Sciences, Guangzhou, Guangdong 510080, China*

Complete contact information is available at: https://pubs.acs.org/10.1021/acsomega.1c03169

Author Contributions

S.C. and L.L. contributed equally to this work. S.C. and L.L.: conceptualization, investigation, methodology, and data curation. M.L., X.C., and M.Y.: supervision, project administration, and data curation. F.P., H.Z., and Y.Z.: supervision, funding acquisition, review, and editing.

Notes

The authors declare no competing financial interest.

■ ACKNOWLEDGMENTS

Financial support from the National Natural Science Foundation of China (52001076), Natural Science Foundation of Guangdong Province, China (2020A1515011447), Scientific and Technological Projects of Guangzhou, China (202002030283 and 202102020431), and Medical Science Foundation of Guangdong Province, China (A2020005) is gratefully acknowledged.

■ REFERENCES

(1) Buling, A.; Zerrer, J. Increasing the application fields of magnesium by ultraceramic: Corrosion and wear protection by plasma electrolytical oxidation (PEO) of Mg alloys. *Surf. Coat. Technol.* **2019**, *369*, 142−155.

(2) Yao, Y.; Chen, L.; Wang, W. Damping Capacities of (B4C+Ti) Hybrid Reinforced Mg and AZ91D Composites Processed by In Situ Reactive Infiltration Technique. *Acta Metall. Sin.* **2019**, *55*, 141−148.

(3) Wang, J.; Pang, X.; Pang, X.; Jahed, H. Surface protection of Mg alloys in automotive applications: A review. *AIMS Mater. Sci.* **2019**, *6*, 567−600.

(4) Li, X.; Liu, X.; Wu, S.; Yeung, K. W. K.; Zheng, Y.; Chu, P. K. Design of magnesium alloys with controllable degradation for biomedical implants: From bulk to surface. *Acta Biomater.* **2016**, *45*, 2−30.

(5) Chen, Y.; Xu, Z.; Smith, C.; Sankar, J. Recent advances on the development of magnesium alloys for biodegradable implants. *Acta Biomater.* **2014**, *10*, 4561−4573.

(6) Zhao, D.; Witte, F.; Lu, F.; Wang, J.; Li, J.; Qin, L. Current status on clinical applications of magnesium-based orthopaedic implants: A review from clinical translational perspective. *Biomaterials* **2017**, *112*, 287−302.

(7) Guo, L.; Wu, W.; Zhou, Y.; Zhang, F.; Zeng, R.; Zeng, J. Layered double hydroxide coatings on magnesium alloys: A review. *J. Mater. Sci. Technol.* **2018**, *34*, 1455.

(8) Yu, J.; Wang, Q.; O'Hare, D.; Sun, L. Preparation of two dimensional layered double hydroxide nanosheets and their applications. *Chem. Soc. Rev.* **2017**, *46*, 5950−5974.

(9) Zhao, M.-Q.; Zhang, Q.; Huang, J.-Q.; Wei, F. Hierarchical Nanocomposites Derived from Nanocarbons and Layered Double Hydroxides - Properties, Synthesis, and Applications. *Adv. Funct. Mater.* **2012**, *22*, 675−694.

(10) Syu, J.-H.; Uan, J.-Y.; Lin, M.-C.; Lin, Z.-Y. Optically transparent Li-Al-CO3 layered double hydroxide thin films on an AZ31 Mg alloy formed by electrochemical deposition and their corrosion resistance in a dilute chloride environment. *Corros. Sci.* **2013**, *68*, 238−248.

(11) Lin, J.-K.; Uan, J.-Y.; Wu, C.-P.; Huang, H.-H. Direct growth of oriented Mg-Fe layered double hydroxide (LDH) on pure Mg substrates and in vitro corrosion and cell adhesion testing of LDH-coated Mg samples. *J. Mater. Chem.* **2011**, *21*, 5011.

(12) Wu, L.; Yang, D.; Zhang, G.; Zhang, Z.; Zhang, S.; Tang, A.; Pan, F. Fabrication and characterization of Mg-M layered double hydroxide films on anodized magnesium alloy AZ31. *Appl. Surf. Sci.* **2018**, *431*, 177−186.

(13) Ye, X.; Jiang, Z.; Li, L.; Xie, Z. H. In-Situ Growth of NiAl-Layered Double Hydroxide on AZ31 Mg Alloy towards Enhanced Corrosion Protection. *Nanomaterials* **2018**, *8*, 411.

(14) Zhou, M.; Yan, L.; Ling, H.; Diao, Y.; Pang, X.; Wang, Y.; Gao, K. Design and fabrication of enhanced corrosion resistance Zn-Al layered double hydroxides films based anion-exchange mechanism on magnesium alloys. *Appl. Surf. Sci.* **2017**, *404*, 246−253.

(15) Peng, F.; Li, H.; Wang, D.; Tian, P.; Tian, Y.; Yuan, G.; Xu, D.; Liu, X. Enhanced Corrosion Resistance and Biocompatibility of Magnesium Alloy by Mg-Al-Layered Double Hydroxide. *ACS Appl. Mater. Interfaces* **2016**, *8*, 35033−35044.

(16) Zhang, D.; Peng, F.; Tan, J.; Liu, X. Y. In-situ growth of layered double hydroxide films on biomedical magnesium alloy by transforming metal oxyhydroxide. *Appl. Surf. Sci.* **2019**, *496*, 143690.
(17) Wu, L. Influence of Reaction Temperature on the Controlled Growth of Mg-Al LDH Film. *Int. J. Electrochem. Sci.* **2017**, *12*, 6352−6364.
(18) Zhang, X.; Zhong, F.; Li, X.; Liu, B.; Zhang, C.; Buhe, B.; Zhang, T.; Meng, G.; Wang, F. The effect of hot extrusion on the microstructure and anti-corrosion performance of LDHs conversion coating on AZ91D magnesium alloy. *J. Alloys Compd.* **2019**, *788*, 756−767.
(19) Wu, L.; Pan, F.; Liu, Y.; Zhang, G.; Tang, A.; Atrens, A. Influence of pH on the growth behaviour of Mg-Al LDH films. *Surf. Eng.* **2018**, *34*, 674−681.
(20) Zhang, G.; Wu, L.; Tang, A.; Zhang, S.; Yuan, B.; Zheng, Z.; Pan, F. A Novel Approach to Fabricate Protective Layered Double Hydroxide Films on the Surface of Anodized Mg-Al Alloy. *Adv. Mater. Interfaces* **2017**, *4*, 1700163.
(21) Zhang, G.; Wu, L.; Tang, A.; Weng, B.; Atrens, A.; Ma, S.; Liu, L.; Pan, F. Sealing of anodized magnesium alloy AZ31 with MgAl layered double hydroxides layers. *RSC Adv.* **2018**, *8*, 2248−2259.
(22) Nakamura, K.; Shimada, Y.; Miyashita, T.; Serizawa, A.; Ishizaki, T. Effect of Vapor Pressure During the Steam Coating Treatment on Structure and Corrosion Resistance of the Mg(OH)(2)/Mg-Al LDH Composite Film Formed on Mg Alloy AZ61. *Materials* **2018**, *11*, 1659.
(23) Kamiyama, N.; Panomsuwan, G.; Yamamoto, E.; Sudare, T.; Saito, N.; Ishizaki, T. Effect of treatment time in the Mg(OH)2/Mg-Al LDH composite film formed on Mg alloy AZ31 by steam coating on the corrosion resistance. *Surf. Coat. Technol.* **2016**, *286*, 172−177.
(24) Chen, J.; Song, Y.; Shan, D.; Han, E.-H. In situ growth of Mg-Al hydrotalcite conversion film on AZ31 magnesium alloy. *Corros. Sci.* **2011**, *53*, 3281−3288.
(25) Chen, J.; Song, Y.; Shan, D.; Han, E.-H. Influence of alloying elements and microstructure on the formation of hydrotalcite film on Mg alloys. *Corros. Sci.* **2015**, *93*, 90−99.
(26) Liu, X.; Zhen, Z.; Liu, J.; Xi, T.; Zheng, Y.; Guan, S.; Zheng, Y.; Cheng, Y. Multifunctional MgF2/Polydopamine Coating on Mg Alloy for Vascular Stent Application. *J. Mater. Sci. Technol.* **2015**, *31*, 733−743.
(27) Mao, L.; Shen, L.; Chen, J.; Wu, Y.; Kwak, M.; Lu, Y.; Xue, Q.; Pei, J.; Zhang, L.; Yuan, G.; Fan, R.; Ge, J.; Ding, W. Enhanced bioactivity of Mg-Nd-Zn-Zr alloy achieved with nanoscale MgF2 surface for vascular stent application. *ACS Appl. Mater. Interfaces* **2015**, *7*, 5320−5330.
(28) Chen, Y.; Zhao, S.; Liu, B.; Chen, M.; Mao, J.; He, H.; Zhao, Y.; Huang, N.; Wan, G. Corrosion-controlling and osteo-compatible Mg ion-integrated phytic acid (Mg-PA) coating on magnesium substrate for biodegradable implants application. *ACS Appl. Mater. Interfaces* **2014**, *6*, 19531−19543.
(29) Asl, V. Z.; Zhao, J. M.; Anjum, M. J.; Wei, S. X.; Wang, W.; Zhao, Z. J. The effect of cerium cation on the microstructure and anti-corrosion performance of LDH conversion coatings on AZ31 magnesium alloy. *J. Alloys Compd.* **2020**, *821*, 153248.
(30) Kuang, J.; Ba, Z.; Li, Z.; Wang, Z.; Qiu, J.; et al. The study on corrosion resistance of superhydrophobic coatings on magensium. *Appl. Surf. Sci.* **2020**, *501*, 144137.
(31) Lin, J.; Hsia, C.; Uan, J. Characterization of Mg,Al-hydrotalcite conversion film on Mg alloy and Cl− and CO32- anion-exchangeability of the film in a corrosive environment. *Scripta Mater.* **2007**, *56*, 927−930.
(32) Tedim, J.; Kuznetsova, A.; Salak, A. N.; Montemor, F.; Snihirova, D.; Pilz, M.; Zheludkevich, M. L.; Ferreira, M. G. S. Zn-Al layered double hydroxides as chloride nanotraps in active protective coatings. *Corros. Sci.* **2012**, *55*, 1−4.
(33) Hu, H.-J.; Liu, X.-Y.; Ding, C.-X. Bioactive Porous and Nanostructured TiO2 Coating Prepared by Plasma Electrolytic Oxidation. *J. Inorg. Mater.* **2011**, *26*, 585−590.
(34) Ding, Z.; Qiao, Y.; Peng, F.; Xia, C.; Qian, S.; Wang, T.; Sun, J.; Liu, X. Si-doped porous TiO2 coatings enhanced in vitro angiogenic behavior of human umbilical vein endothelial cells. *Colloids Surf., B* **2017**, *159*, 493−500.
(35) Kusumbe, A. P.; Ramasamy, S. K.; Adams, R. H. Coupling of angiogenesis and osteogenesis by a specific vessel subtype in bone. *Nature* **2014**, *507*, 323−328.
(36) Xie, H.; Cui, Z.; Wang, L.; Xia, Z.; Hu, Y.; Xian, L.; Li, C.; Xie, L.; Crane, J.; Wan, M.; Zhen, G.; Bian, Q.; Yu, B.; Chang, W.; Qiu, T.; Pickarski, M.; Duong, L. T.; Windle, J. J.; Luo, X.; Liao, E.; Cao, X. PDGF-BB secreted by preosteoclasts induces angiogenesis during coupling with osteogenesis. *Nat. Med.* **2014**, *20*, 1270−1278.
(37) He, W.; Zhang, H.; Qiu, J. X. Osteogenic effects of bioabsorbable magnesium implant in rat mandibles and in vitro. *J. Periodontol.* **2020**, DOI: 10.1002/JPER.20-0162.
(38) Kawamura, N.; Nakao, Y.; Ishikawa, R.; Tsuchida, D.; Iijima, M. Degradation and Biocompatibility of AZ31 Magnesium Alloy Implants In Vitro and In Vivo: A Micro-Computed Tomography Study in Rats. *Materials* **2020**, *13*, 473.
(39) Peng, F.; Wang, D. H.; Tian, Y. X.; Cao, H. L.; Qiao, Y. Q.; Liu, X. Y. Sealing the Pores of PEO Coating with Mg-Al Layered Double Hydroxide: Enhanced Corrosion Resistance, Cytocompatibility and Drug Delivery Ability. *Sci. Rep.* **2017**, *7*, 8167.

https://doi.org/10.1021/acsomega.1c03169
ACS Omega 2021, 6, 24575−24584